نشریه ژئومکانیک و ژئوانرژی (ژئومکانیک نفت)

GEOMECHANICS and GEOENERGY JOURNAL (GGJ)

Original article

Thermo-Mechanical Behavior of Graphene-Reinforced Auxetic Sandwich Beams as an Equivalent Model for Oil-Well Casing Subjected to Geomechanical Loading

Armin Khoddami[1], Akbar Alibeigloo[1*]

1- Department of Mechanical Engineering, Tarbiat Modares University, Tehran , Iran

Received: 2025/07/30; Accepted: 2026/03/16
DOI: 10.22107/ggj.2026.594483.1269

Keywords

Graphene nanoplatelets (GPLs), Auxetic sandwich beam, Geomechanical loading, Oil-well casing, Thermo-mechanical stability, Structural buckling

Abstract

Oil-well casing structures operating in deep underground environments are simultaneously subjected to high geomechanical stresses and elevated temperatures, which may significantly reduce their structural stability and service life. This study presents a unified analytical framework for evaluating the thermo-mechanical behavior of advanced oil-well casing systems using an equivalent graphene nanoplatelet-reinforced composite (GPLRC) sandwich beam with a re-entrant auxetic core. The proposed model is formulated based on Reddy's third-order shear deformation theory, Hamilton's principle, and the Navier solution to investigate the bending and buckling responses under coupled geomechanical and thermal loading conditions. Temperature-dependent material properties, effective in-situ geomechanical stresses, and thermally induced compressive forces are incorporated into the formulation to realistically represent downhole operating conditions. A comprehensive parametric study is conducted to examine the influences of GPL volume fraction, GPL distribution pattern, auxetic cell angle, geomechanical loading, and temperature on the structural performance of the equivalent casing model. The results demonstrate that increasing the GPL content from 0 to 1% reduces the mid-span deflection by approximately 68% and increases the critical buckling load by about 212%, while the FG-X distribution provides the best overall structural performance. The proposed configuration reaches the adopted linear-response limit at an effective external pressure of approximately 48.5 MPa, and thermo-mechanical buckling occurs at a critical temperature rise of about 242 °C for the highest investigated preload ratio. The findings demonstrate that the combined use of GPL-reinforced face sheets and a re-entrant auxetic core can significantly enhance the stiffness and global stability characteristics of the proposed equivalent sandwich-beam model. Furthermore, the developed analytical framework provides a computationally efficient reduced-order tool for preliminary parametric assessment of casing-related global response modes under representative high-pressure and high-temperature downhole conditions.

1. Introduction

Ensuring the structural integrity of oil-well casing becomes increasingly challenging in deep and ultra-deep wells, where the wellbore system may be subjected to complex combinations of in-situ stresses, pore pressure, internal wellbore pressure, and temperature variations. These coupled geomechanical and thermo-mechanical effects can significantly influence wellbore stability and the mechanical response of the casing during drilling and production operations [1]. Previous studies have shown that stress redistribution and thermo-hydro-mechanical coupling around the wellbore can lead to considerable changes in deformation and stability, highlighting the importance of developing efficient mechanical models for assessing structural response under representative downhole loading conditions [2,3].

*** Corresponding Author:** abeigloo@modares.ac.ir

Sandwich structures provide high bending rigidity and structural efficiency through the combination of relatively stiff face sheets and a lightweight core. Their mechanical behavior can be further tailored by modifying the geometry and material characteristics of the core. Among different cellular configurations, re-entrant auxetic honeycombs have attracted particular attention because of their negative Poisson's ratio and distinctive deformation mechanisms. Such cellular architectures can exhibit enhanced shear resistance, indentation resistance, energy absorption, and structural stability compared with conventional cellular configurations [4–6]. Experimental and numerical investigations have further demonstrated that the cell angle and geometrical parameters of re-entrant honeycombs can considerably affect the bending response, load-carrying capacity, and stability of sandwich structures [7].

Graphene nanoplatelets (GPLs) represent another promising means of tailoring the mechanical properties of advanced composite structures. Owing to their high elastic modulus and favorable thermo-mechanical characteristics, small quantities of GPLs can significantly modify the effective stiffness of polymer-based composites [8]. In addition to the reinforcement content, the spatial distribution of GPLs through the thickness plays an important role in controlling structural performance. Tam et al. [9] demonstrated that GPL distribution significantly influences the vibration and buckling characteristics of functionally graded composite beams, while Arefi and Najafitabar [10] reported considerable effects of functionally graded GPL-reinforced face sheets on the buckling and free-vibration behavior of sandwich beams. These findings indicate that both the amount and distribution of GPL reinforcement should be considered when designing sandwich configurations for enhanced bending and stability performance.

Several recent investigations have combined auxetic architectures with graphene-reinforced materials to study their response under mechanical and thermal loading. Nguyen et al. [4] performed a comprehensive analysis of auxetic honeycomb sandwich plates with GPL-reinforced face sheets and showed that both GPL distribution and auxetic-cell geometry have significant effects on buckling and dynamic instability. Wang et al. [11] investigated the thermal postbuckling behavior of sandwich beams with functionally graded auxetic graphene-reinforced cores and demonstrated the sensitivity of structural stability to core characteristics and temperature. Lieu et al. [5] studied the static bending and buckling of functionally graded sandwich nanobeams with auxetic honeycomb cores and reported notable effects of cell geometry, material gradation, and boundary conditions. Related thermo-mechanical studies on auxetic graphene-reinforced sandwich plates and cylindrical shells have also confirmed that temperature, reinforcement distribution, and structural geometry can strongly influence stability and postbuckling behavior [12–14]. More recently, the response of GPL-reinforced auxetic cylindrical sandwich structures subjected to thermal and external-pressure environments has further highlighted the potential of such material architectures for stability-sensitive structural applications [15].

In parallel, petroleum-geomechanics research has extensively addressed wellbore stability, stress redistribution, and the response of conventional well systems under in-situ stress, pore-pressure, thermal, and pressure-loading conditions [16]. However, most such investigations are based on continuum wellbore or conventional casing representations, whereas studies on graphene-reinforced auxetic structures have predominantly focused on conventional beam, plate, and shell applications [4,5,10–15]. Consequently, a direct connection between these two research areas remains limited, particularly for reduced-order models intended to examine the global longitudinal bending and compressive-stability response of an equivalent casing structure under representative geomechanical and thermal loading.

Accordingly, the present study develops an equivalent GPL-reinforced sandwich beam with a re-entrant auxetic core to represent the global longitudinal structural response of an oil-well casing. The analytical formulation is established using Reddy's third-order shear deformation theory, Hamilton's principle, and the Navier solution. The effects of GPL volume fraction, GPL distribution pattern, auxetic-cell angle, effective geomechanical pressure, initial axial preload, and temperature rise on the bending and buckling responses are systematically investigated. The proposed representation is intended as a reduced-order analytical framework for preliminary structural assessment and parametric investigation of the selected global response modes; it is not intended to reproduce local three-dimensional casing phenomena such as circumferential ovalization, threaded connections, cement–casing interaction, or localized material damage.

2. Mathematical Formulation

2.1. Equivalent Oil-Well Casing Model

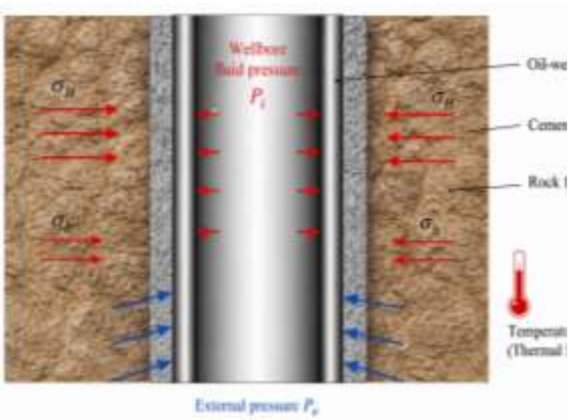

Fig.1. Schematic representation of an oil-well casing subjected to representative geomechanical and thermo-mechanical loading conditions.

The proposed equivalent modeling strategy is established to investigate the thermo-mechanical behavior of an oil-well casing subjected to representative geomechanical loading conditions. As illustrated in Fig.1, the casing installed in a deep geological formation is simultaneously subjected to in-situ geomechanical stresses, internal wellbore pressure, external formation pressure, and temperature variations generated during drilling and production operations. The combined action of these loading components continuously alters the stress state of the casing and may eventually result in excessive deformation, structural instability, or failure during long-term service.

The structural response of the casing is mainly governed by the interaction between the maximum and minimum horizontal in-situ stresses (σH,σh), the internal wellbore pressure (P_i), the external formation pressure (P_e), and the temperature increment (ΔT). These coupled thermo-mechanical and geomechanical actions produce a complex stress field that significantly influences the load-carrying capacity, structural stability, and durability of the casing throughout its operational lifetime.

Although the casing is essentially a cylindrical shell, its dominant longitudinal structural behavior can be effectively represented using an equivalent beam model. Such a reduced-order representation considerably simplifies the mathematical formulation while preserving the principal mechanical characteristics associated with global bending and compressive buckling under coupled thermo-mechanical loading conditions.

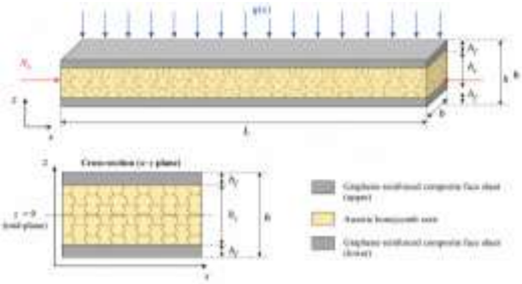

Fig.2. Equivalent graphene-reinforced auxetic sandwich beam model representing the longitudinal structural response of the oil-well casing.

The equivalent structural model adopted in the present study is illustrated in Fig. 2, representative longitudinal strip of the cylindrical casing is idealized as a three-layer graphene-reinforced auxetic sandwich beam consisting of two graphene nanoplatelet-reinforced composite face sheets bonded to an auxetic honeycomb core. The upper and lower face sheets primarily resist the normal stresses induced by bending, whereas the auxetic core transfers transverse shear stresses and contributes to the flexural stiffness and buckling resistance of the equivalent structure.

The equivalent sandwich beam has length L, width b, total thickness h, core thickness h_c, and identical upper and lower face-sheet thicknesses h_f. A Cartesian coordinate system (x, z) is adopted, where the x-axis is aligned with the longitudinal direction of the beam and the z-axis is measured through the thickness from the mid-plane of the sandwich structure. The surrounding formation and wellbore pressure state are transformed into an equivalent transverse geomechanical line load $q_{geo}(x)$ acting on the representative longitudinal casing strip. The axial geomechanical action employed in the buckling analysis is treated separately as an initial compressive resultant N_{geo}, while a uniform temperature increment ΔT is introduced to account for the thermal conditions encountered during drilling and production operations. The detailed transformation of the geomechanical stress and pressure components into the equivalent beam loads is presented below.

2.1.1 Transformation of the Geomechanical Loading

To establish a direct physical connection between the actual downhole stress state and the reduced-order beam model, the horizontal in-situ stresses are first converted into effective stresses by incorporating the formation pore pressure through Biot's effective-stress concept. Accordingly, the maximum and minimum effective horizontal stresses are expressed as

$$\sigma'_H = \sigma_H - \alpha_B P_p \quad , \; \sigma'_h = \sigma_h - \alpha_B P_p \qquad (1)$$

where P_p is the formation pore pressure and α_B denotes the Biot coefficient. At a circumferential position θ, measured from the direction of the maximum horizontal stress, the effective external normal pressure acting on the representative casing strip is obtained from the transformation of the horizontal stress field as

$$P_{ext}(\theta) = \sigma'_H cos^2\theta + \sigma'_h sin^2\theta \qquad (2)$$

The net inward pressure acting on the casing is subsequently determined by accounting for the internal wellbore pressure P_i :

$$P_{net} = \max\,[P_{ext}(\theta) - P_{i,} 0] \qquad (3)$$

For a representative longitudinal casing strip of width b, the corresponding transverse line load employed in the equivalent beam formulation is

$$q_{geo}(x) = P_{net}\; b \qquad (4)$$

In the present geomechanical pressure analysis, $\theta = 0 \circ$ is considered, such that $P_{ext} = \sigma_H - \alpha_B P_p$.The longitudinal geomechanical action used in the buckling analysis is represented independently by an initial compressive resultant $N_{geo} = \mu N_{cr,0}$ where $N_{cr,0}$ is the critical buckling load at the reference temperature and μ denotes the prescribed preload ratio.
The proposed equivalent beam model is intended to reproduce the global longitudinal thermo-mechanical response of the casing rather than its complete three-dimensional cylindrical behavior. Therefore, local effects such as circumferential ovalization, threaded casing connections, cement–casing interaction, and localized material damage are not considered in the present formulation. The adopted model provides a computationally efficient framework for developing the analytical relations presented in the subsequent.

2.2. Geometry of the Auxetic Honeycomb core

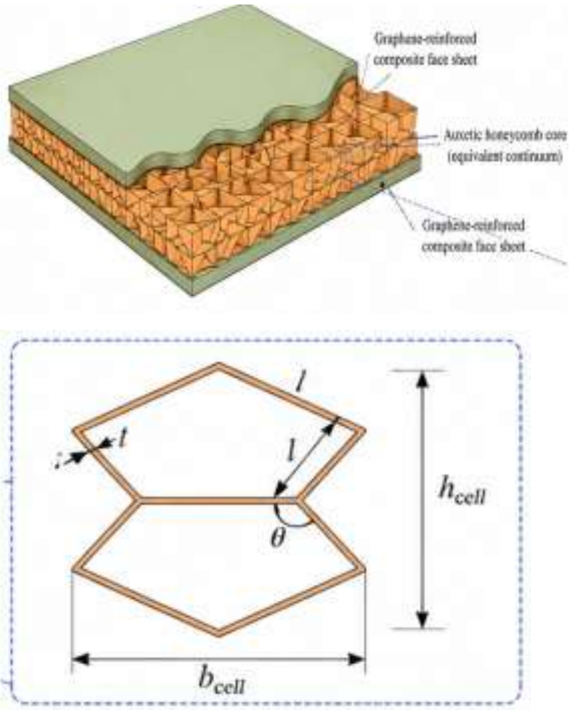

Fig. 3. Geometry of the re-entrant auxetic honeycomb unit cell and its geometrical parameters.

The mechanical performance of sandwich structures is strongly influenced by the geometrical configuration of the core. In the present study, a re-entrant auxetic honeycomb is employed as the core layer of the equivalent sandwich beam owing to its negative Poisson's ratio, excellent shear resistance, and enhanced structural stability. Compared with conventional honeycomb cores, the re-entrant cellular topology exhibits a unique deformation mechanism that improves the bending stiffness, buckling resistance, and energy absorption capability of sandwich structures subjected to combined thermo-mechanical loading conditions .

The re-entrant angle (θ) governs the deformation mechanism of the cellular structure and is the primary parameter responsible for the negative Poisson's ratio. Variations in (θ) modify the relative density, equivalent Young's modulus, equivalent shear modulus, and effective Poisson's ratio of the auxetic core. Likewise, the wall thickness (t), together with the characteristic lengths (l) and (h), significantly influences the bending rigidity and transverse shear stiffness of the equivalent sandwich beam. Consequently, the global bending and buckling behavior of the equivalent oil-well casing strongly depends on the geometrical characteristics of the re-entrant honeycomb unit cell.

For the present formulation, the auxetic core is assumed to consist of periodically repeated identical unit cells with uniform wall thickness. Furthermore, perfect bonding between the graphene nanoplatelet-reinforced composite face sheets and the auxetic honeycomb core is assumed, ensuring full displacement compatibility at the interfaces. These assumptions are commonly adopted in the theoretical modeling of auxetic sandwich structures and provide a suitable basis for deriving the equivalent mechanical properties of the core.

The equivalent mechanical properties of the auxetic honeycomb are subsequently determined using an equivalent continuum approach based on the geometrical characteristics of the representative unit cell. These effective properties are then incorporated into the constitutive formulation of the equivalent graphene-reinforced sandwich beam presented in the following section.

2.3. Effective Material Properties of the Auxetic Honeycomb Core

The re-entrant auxetic honeycomb is modeled as an equivalent homogeneous orthotropic continuum. In this approach, the mechanical behavior of the periodic cellular core is represented by equivalent elastic constants determined from the geometry of the representative unit cell shown in Fig.3 and the properties of the solid cell-wall material. The cell-wall material is assumed to be homogeneous, isotropic, and linearly elastic, with Young's modulus E_s, Poisson's ratio ν_s, and density ρ_s.

2.3.1. Relative Density

The relative density represents the amount of solid material contained within the cellular structure and significantly affects the stiffness and strength of the auxetic core. For the re-entrant unit cell shown in Fig. 3, the relative density is expressed as

$$\frac{\rho_c}{\rho_s} = \frac{t(2l+h)}{2l\cos\theta(h-l\sin\theta)} \tag{5}$$

where ρc is the equivalent density of the auxetic core, ρ_s is the density of the solid cell-wall material, t is the cell-wall thickness, l is the inclined wall length, h is the vertical wall length, and θ is the re-entrant angle.

Equation (5) shows that the equivalent density is governed by the unit-cell geometry. Increasing the wall thickness t increases the relative density, whereas increasing the characteristic cell dimensions generally reduces the amount of solid material within the cellular structure. The re-entrant angle also modifies the projected dimensions of the unit cell and consequently affects the effective mechanical properties of the core.

2.3.2. Equivalent Young's Moduli

The deformation of the re-entrant honeycomb is mainly governed by bending of the inclined cell walls. Therefore, the equivalent elastic moduli strongly depend on the wall slenderness ratio and the geometrical configuration of the unit cell.

The equivalent Young's modulus in the x-direction is given by

$$\frac{E_x}{E_s} = \left(\frac{t}{l}\right)^3 \frac{\cos\theta}{\left(\frac{h}{l}+\sin\theta\right)\sin^2\theta} \tag{6}$$

The equivalent Young's modulus in the y-direction is expressed as

$$\frac{E_y}{E_s} = \left(\frac{t}{l}\right)^3 \frac{\left(\frac{h}{l}+\sin\theta\right)\sin^2\theta}{\cos^3\theta} \tag{7}$$

where E_s denotes the Young's modulus of the solid cell-wall material, while E_x, E_y, and G_{xy} are the effective elastic moduli of the auxetic core. Accordingly, Eqs. (6)–(8) are expressed in normalized form with respect to Es, ensuring dimensional consistency. These relations are based on the equivalent continuum formulation for cellular honeycomb structures [17].

2.3.3. Equivalent Shear Modulus

The equivalent shear modulus is an important parameter in the bending and buckling analysis of sandwich beams, particularly when a higher-order shear deformation theory is employed. It is expressed as

$$\frac{G_{xy}}{E_s} = \left(\frac{t}{l}\right)^3 \frac{\left(\frac{h}{l}+sin\theta\right)}{(\frac{h}{l})^2(1+2sin^2\theta)cos\theta} \tag{8}$$

where G_{xy} denotes the effective in-plane shear modulus of the auxetic core.

Equation (8) demonstrates that the shear stiffness is also highly dependent on the cell-wall slenderness ratio and the re-entrant geometry. This parameter directly influences the transverse shear rigidity of the sandwich beam and therefore affects both its bending deformation and critical buckling load.

2.3.4. Equivalent Poisson's Ratio

The negative Poisson's ratio is the main characteristic of re-entrant auxetic structures. Under longitudinal tension, the cell walls rotate and cause lateral expansion, whereas under compression, lateral contraction occurs.

The equivalent Poisson's ratio is given by

$$\nu_{xy} = -\frac{cos^2\theta}{\left(\frac{h}{l}+sin\theta\right)sin\theta} \tag{9}$$

where ν_{xy} is the effective Poisson's ratio of the auxetic core.

Equation (9) indicates that the auxetic behavior is controlled by the geometrical configuration of the unit cell. The negative sign represents the lateral expansion of the core under axial tension. By changing the re-entrant angle and the ratio h/l, the magnitude of the negative Poisson's ratio can be adjusted, allowing the mechanical response of the sandwich beam to be tailored.

2.4. Effective Material Properties of Graphene-Reinforced Composite Face Sheets

The face sheets of the equivalent sandwich beam are assumed to be fabricated from graphene nanoplatelet-reinforced composite (GPLRC) materials. Due to the exceptional stiffness and thermal stability of graphene nanoplatelets (GPLs), the incorporation of GPLs into the polymer matrix significantly enhances the mechanical and thermo-mechanical performance of the composite face sheets. In the present study, the effective material properties of the GPLRC face sheets are evaluated using the modified Halpin–Tsai micromechanical model in conjunction with the rule of mixtures. This approach provides accurate predictions of the effective elastic properties while maintaining computational efficiency for the subsequent analytical formulation.

2.4.1. GPL Distribution Patterns

In the present study, the functionally graded X-type (FG-X) distribution pattern is adopted for the graphene nanoplatelet-reinforced composite face sheets. In this distribution, the graphene nanoplatelets (GPLs) are symmetrically distributed along the thickness direction of the face sheet, with a higher concentration near the outer surfaces and a lower concentration at the mid-plane, as illustrated in Fig.4.

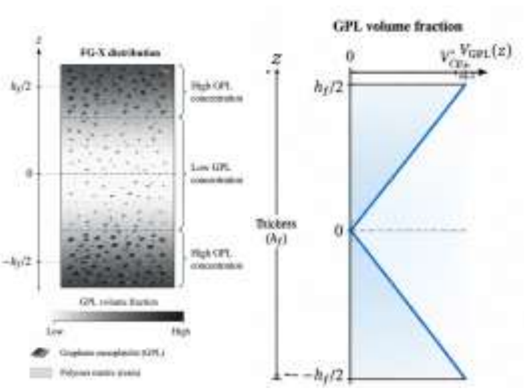

Fig. 4. Schematic illustration of the FG-X distribution pattern of graphene nanoplatelets through the thickness of the composite face sheet

The GPL volume fraction through the thickness direction is defined as

$$V_{GPL}(z) = V_{GPL}^{*} \frac{2|z|}{h_f} \tag{10}$$

where $V_{GPL}(z)$ denotes the local GPL volume fraction at the thickness coordinate z, V_{GPL}^{*} represents the maximum GPL volume fraction, and h_f is the thickness of the composite face sheet.

This distribution function indicates that the GPL concentration increases linearly from the mid-plane toward both outer surfaces of the face sheet. The obtained GPL volume fraction is subsequently used to determine the effective elastic and thermal properties of the graphene-reinforced composite face sheets.

2.4.2. Effective Elastic Properties

The effective elastic properties of the graphene nanoplatelet-reinforced composite face sheets are evaluated using the modified Halpin–Tsai micromechanical model. The GPL volume fraction distribution obtained from Eq. (10) is employed to determine the variation of the composite properties along the thickness direction.

The local GPL volume fraction is first converted from the weight fraction using

$$V_{GPL}^{*} = \frac{W_{GPL}/\rho_{GPL}}{\frac{W_{GPL}}{\rho_{GPL}}+W_m/\rho_m} \tag{11}$$

Where W_{GPL} and W_m represent the weight fractions of GPLs and the matrix material, respectively. The matrix volume fraction is obtained as

$$V_m(z) = 1 - V_{GPL}(z) \tag{12}$$

The effective Young's modulus of the GPL-reinforced composite face sheet is determined using the modified Halpin–Tsai model as

$$E_f(z) = \frac{3}{8}E_L(z) + \frac{5}{8}E_T(z) \tag{13}$$

where $E_L(z)$ and $E_T(z)$ are the longitudinal and transverse Young's moduli, respectively, which are expressed as

$$E_L(z) = E_m \frac{1+\xi_L \eta_L V_{GPL}(z)}{1-\eta_L V_{GPL(z)}} \tag{14}$$

$$E_T(z) = E_m \frac{1+\xi_T \eta_T V_{GPL}(z)}{1-\eta_T V_{GPL(z)}} \tag{15}$$

where E_m is the Young's modulus of the polymer matrix, and ξ_L and ξ_T are the shape parameters associated with the GPL geometry. The parameters η_L and η_T are defined as

$$\eta_L = \frac{\frac{E_{GPL}}{E_m}-1}{\frac{E_{GPL}}{E_m}+\xi_L} \tag{16}$$

$$\eta_T = \frac{\frac{E_{GPL}}{E_m}-1}{\frac{E_{GPL}}{E_m}+\xi_T} \tag{17}$$

The effective shear modulus, Poisson's ratio, and density of the GPL-reinforced composite face sheet are subsequently calculated as

$$G_f(z) = \frac{E_f(z)}{2(1+\nu_f(z))} \tag{18}$$

$$\nu_f(z) = \nu_{GPL} V_{GPL}(z) + \nu_m V_m(z) \tag{19}$$

$$\rho_f(z) = \rho_{GPL} V_{GPL}(z) + \rho_m V_m(z) \tag{20}$$

where $\nu_f(z)$ and $\rho_f(z)$ denote the effective Poisson's ratio and density of the GPL-reinforced composite face sheet, respectively.

2.4.3. Effective Thermal Expansion Coefficient

The thermal expansion behavior of the GPL-reinforced composite face sheets is considered through the effective coefficient of thermal expansion. Since the GPL distribution varies along the thickness direction, the thermal expansion coefficient is also assumed to be thickness-dependent. The effective thermal expansion coefficient is evaluated using the rule of mixtures as

$$\alpha_f(z) = \frac{\alpha_{GPL} V_{GPL}(z) E_{GPL} + \alpha_m V_m(z) E_m}{V_{GPL}(z) E_{GPL} + V_m(z) E_m} \tag{21}$$

where $\alpha_f(z)$ denotes the effective thermal expansion coefficient of the GPL-reinforced composite face sheet. The parameters α_{GPL} and α_m represent the thermal expansion coefficients of graphene nanoplatelets and the polymer matrix, respectively.

2.5. Displacement Field Based on Reddy's Third-Order Shear Deformation Theory

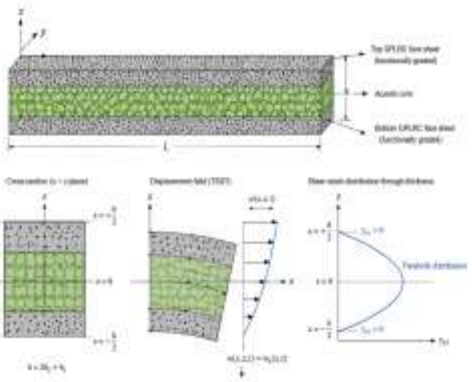

Fig. 5. Sandwich beam displacement and strain distribution

The sandwich beam considered in the present study consists of two graphene nanoplatelet-reinforced composite (GPLRC) face sheets and an auxetic honeycomb core, as illustrated in Fig. 5. The coordinate system is defined such that the x-axis represents the longitudinal direction of the beam, while the z-axis is measured along the thickness direction. The total thickness of the sandwich beam is expressed as $h = 2h_f + h_c$, where h_f and h_c denote the thicknesses of the face sheets and the auxetic core, respectively.
To consider the transverse shear deformation effects, Reddy's third-order shear deformation theory (TSDT) is adopted. Unlike the classical beam theory, TSDT introduces a higher-order variation of the displacement field through the thickness direction and satisfies the zero transverse shear stress conditions at the top and bottom surfaces of the beam without requiring any shear correction factor.
According to the TSDT formulation, the displacement field of an arbitrary point within the sandwich beam is defined as

$$u(x, z, t) = u_0(x, t) - z\frac{\partial \omega_0(x,t)}{\partial x} + \left(z - \frac{4z^3}{3h^2}\right)\phi(x, t) \tag{22}$$

$$\omega(x, z, t) = \omega_0(\mathrm{x}, \mathrm{t}) \tag{23}$$

Where $u(x, z, t)$ and $\omega(x, z, t)$ represent the longitudinal and transverse displacements of an arbitrary point within the beam, respectively. The variables $u_0(x, t)$ and $\omega_0(x, t)$ denote the axial and transverse displacements of the reference surface $(z = 0)$, while $\phi(x, t)$ represents the independent rotation of the cross-section.
The cubic term in Eq. (23) results in a parabolic distribution of the transverse shear strain through the thickness direction, as shown in Fig. 5. Therefore, the transverse shear strain becomes zero at the upper and lower surfaces of the beam, satisfying the required stress-free boundary conditions. The adopted TSDT formulation is consequently capable of accurately predicting the bending and buckling behavior of the GPLRC/auxetic core/GPLRC sandwich beam subjected to thermo-mechanical loading conditions.

2.6. Strain–Displacement Relations

Based on the displacement field defined by Reddy's third-order shear deformation theory, the longitudinal normal strain and transverse shear strain are obtained from the linear strain–displacement relations. These strain components are employed in the subsequent constitutive formulation and governing equations.
The axial normal strain is given by

$$\varepsilon_x = \frac{\partial u}{\partial x} \tag{24}$$

and the transverse shear strain is expressed as

$$\gamma_{xz} = \frac{\partial u}{\partial z} + \frac{\partial \omega}{\partial x} \tag{25}$$

Substituting Eqs. (24) and (25) into the above relations yields

$$\varepsilon_x = \frac{\partial u_0}{\partial x} - z\frac{\partial^2 \omega_0}{\partial x^2} + \left(z - \frac{4z^3}{3h^2}\right)\frac{\partial \phi}{\partial x} \tag{26}$$

$$\gamma_{xz} = \left(1 - \frac{4z^2}{h^2}\right)\phi \tag{27}$$

where ε_x denotes the longitudinal normal strain and γ_{xz} represents the transverse shear strain. It can be observed that the transverse shear strain follows a parabolic distribution through the beam thickness and automatically satisfies the zero shear stress condition at the upper and lower surfaces of the sandwich beam. Consequently, the adopted strain field is well suited for the thermo-mechanical analysis of GPLRC/auxetic sandwich beams.

2.7. Constitutive Equations

The constitutive equations of the GPLRC/auxetic sandwich beam are established based on the linear thermoelastic theory. Both the graphene nanoplatelet-reinforced composite (GPLRC) face sheets and the auxetic honeycomb core are assumed to behave as linear elastic materials. The thermal effect is incorporated through the thermal strain associated with the applied temperature variation.

The constitutive relation of each layer can be expressed as

$$\sigma = Q(\epsilon - \varepsilon^T) \tag{28}$$

where the thermal strain vector is given by

$$\varepsilon^T = \alpha(Z)\Delta T \tag{29}$$

in which $\alpha(Z)$ denotes the effective coefficient of thermal expansion and ΔT represents the temperature increment.

For the present one-dimensional beam formulation, the constitutive matrix is written as

$$Q = \begin{bmatrix} Q_{11} & 0 \\ 0 & Q_{55} \end{bmatrix} \tag{30}$$

The material stiffness coefficients for the GPLRC face sheets are

$$Q_{11} = E_f(z) \tag{31}$$

$$Q_{55} = G_f(z) \tag{32}$$

where $E_f(z)$ and $G_f(z)$ are the effective Young's modulus and shear modulus obtained from the modified Halpin–Tsai model.

Similarly, the constitutive coefficients of the auxetic honeycomb core are expressed as

$$Q_{11} = E_C \tag{33}$$

$$Q_{55} = G_C \tag{34}$$

where E_C and G_C denote the equivalent Young's modulus and shear modulus of the auxetic honeycomb core derived in Section 2.3.

Accordingly, the normal and transverse shear stresses are written as

$$\sigma_x = Q_{11}(\varepsilon_x - \alpha(z)\Delta T) \tag{35}$$

$$\tau_{xz} = Q_{55}\gamma_{xz} \tag{36}$$

The above constitutive equations provide the thermoelastic relationship between the stress and strain components of the GPLRC face sheets and the auxetic honeycomb core. These equations are subsequently employed in the evaluation of the strain energy and the derivation of the governing equations for the thermo-mechanical bending and buckling analysis of the sandwich beam.

2.8. Governing Equations Based on Hamilton's Principle

The governing equations of the GPLRC/auxetic sandwich beam are derived based on Hamilton's principle. According to this principle, the dynamic equilibrium of the system is established by requiring the first variation of the total energy functional to vanish over the time interval [t1 , t2] which can be expressed as

$$\delta = \int_{t_1}^{t_2}(U + W_T - T - W)\,dt = 0 \tag{37}$$

where U, W_T , T, and W denote the strain energy, thermal potential energy, kinetic energy, and the work performed by the external mechanical loads, respectively.

The strain energy of the sandwich beam is defined as

$$U = \frac{1}{2}\int_V(\sigma_x\varepsilon_x + \tau_{xz}\gamma_{xz})\,dV \tag{38}$$

where the stress components are determined from the constitutive equations presented in Section 2.7.

The thermal potential energy associated with the temperature variation is given by

$$W_T = \int_V \sigma_x^T\varepsilon_x\,dV \tag{39}$$

where the thermal stress is expressed as

$$\sigma_x^T = E(z)\alpha(z)\Delta T \tag{40}$$

The kinetic energy of the sandwich beam is written as

$$T = \frac{1}{2}\int_V \rho(z)(\dot{u}^2 + \dot{\omega}^2)\, dV \quad (41)$$

where $\rho(z)$ denotes the effective mass density through the beam thickness.
The work done by the external transverse load is expressed as

$$W = \int_0^L q(x)\omega(x)dx \quad (42)$$

where $q(x)$ is the distributed transverse load acting along the beam length.
Substituting Eqs. (39)–(42) into Eq. (38) and applying the variational procedure yield the governing differential equations together with the corresponding natural boundary conditions of the GPLRC/auxetic sandwich beam under thermo-mechanical loading. These governing equations constitute the basis for the subsequent bending and buckling analyses.

2.9. Navier Solution Procedure

For a simply supported GPLRC/auxetic sandwich beam, the governing equations derived from Hamilton's principle are solved using Navier's solution method. In this method, the generalized displacement variables are expanded into trigonometric series that automatically satisfy the simply supported boundary conditions.
Accordingly, the displacement variables are assumed as

$$u_0(x) = \sum_{m=1}^{\infty} U_m \cos\left(\frac{m\pi x}{L}\right) \quad (43)$$

$$\omega_0(x) = \sum_{m=1}^{\infty} W_m \sin\left(\frac{m\pi x}{L}\right) \quad (44)$$

$$\phi(x) = \sum_{m=1}^{\infty} \Phi_m \cos\left(\frac{m\pi x}{L}\right) \quad (45)$$

where U_m,W_m , and Φ_m are the unknown modal coefficients, L is the beam length, and m denotes the mode number.
Substituting Eqs. (43)–(45) into the governing equations and utilizing the orthogonality properties of the trigonometric functions transforms the governing partial differential equations into a system of algebraic equations for each mode.
For the static bending analysis, the resulting system is expressed as

$$Kd = F \quad (46)$$

where K is the stiffness matrix, F is the generalized load vector, and the generalized displacement vector is defined as

$$\text{Where : } d = \begin{Bmatrix} U_m \\ W_m \\ \Phi_m \end{Bmatrix} \quad (47)$$

For the thermo-mechanical buckling analysis, the governing equations are converted into the following eigenvalue problem

$$(K - \lambda K_G)\, d = 0 \quad (48)$$

where K_G represents the geometric stiffness matrix induced by the thermo-mechanical loading and λ\lambdaλ is the buckling load parameter.
The critical buckling load is obtained from the minimum positive eigenvalue of Eq. (48), while the corresponding eigenvector represents the associated buckling mode shape. The static bending response is obtained by solving Eq. (46).
The developed formulation is implemented in MATLAB to evaluate the thermo-mechanical bending response and buckling behavior of the GPLRC/auxetic sandwich beam under different material, geometric, and thermal loading conditions.

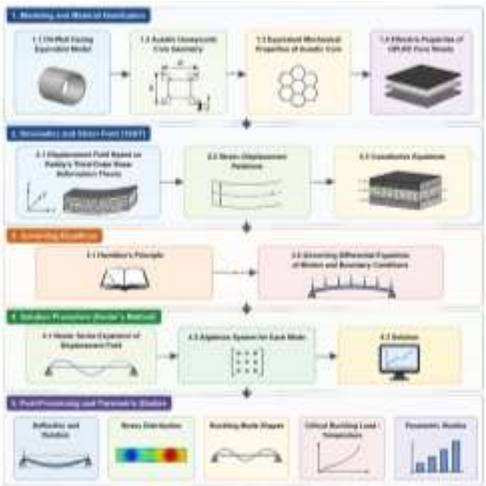

Fig. 6. Overall analytical framework of the present thermo-mechanical bending and buckling analysis**.**

The principal geometric, material, thermal, and loading parameters employed in the numerical analyses are summarized in Table 1.

Table 1 Geometric, material, and loading parameters used in the numerical analyses.

parameter	symbol	value
Casing outer diameter	D_o	244.5 mm
Equivalent unsupported length	L	32.826 mm
Equivalent strip width	b	20.289 mm
Total sandwich thickness	h	12 mm
Face-sheet thickness	h_f	1.5 mm
Auxetic-core thickness	h_c	9 mm
Circumferential strip angle	$\Delta\emptyset$	10°
Epoxy Young's modulus	E_{mo}	3.0 GPa
Epoxy Poisson's ratio	υ_m	0.34
Epoxy density	ρ_m	1200 kg/m³
Epoxy thermal expansion coefficient	α_m	$45*10^{-6}$ k^{-1}
GPL Poisson's ratio	υ_g	0.186
GPL thermal expansion coefficient	α_g	$5*10^{-6}$ K^{-1}
Halpin–Tsai parameters	ξ_L , ξ_W	3333.33 , 2000
Core solid Young's modulus	E_{s0}	70 GPa
Core solid shear modulus	G_{s0}	27 GPa
Core solid density	ρ_s	2700 kg/m³
Core thermal expansion coefficient	α_s	$23*10^{-6}$ k^{-1}
Minimum horizontal stress	σ_h	45 MPa
Formation pore pressure	P_p	25 MPa
Internal wellbore pressure	P_i	20 MPa
Temperature rise	ΔT	0–300 °C

The auxetic unit-cell geometry is defined through the dimensionless ratios h_0/l_0 and t/l_0, since the equivalent core properties depend on the normalized cell geometry. The Halpin–Tsai parameters are determined from the GPL dimensions as $\xi_L = 2l_g/t_g$ and $\xi_w = 2w_g/t_g$. The thermal formulation is expressed in terms of the temperature rise ΔT, with $\Delta T = 0$ representing the reference material state.

3. Results and Discussion

This section presents and discusses the numerical results obtained from the developed TSDT–Navier model. The convergence and accuracy of the solution are first examined, followed by parametric investigations into the effects of GPL reinforcement, auxetic-core geometry, geomechanical loading, and temperature on the bending and buckling responses of the equivalent oil-well casing model.

3.1. Numerical Convergence and Model Validation

Prior to the parametric analyses, the convergence and accuracy of the developed numerical formulation were examined. The convergence of the Navier-series solution was evaluated using the mid-span deflection of the simply supported GPLRC–auxetic sandwich beam, while the buckling formulation was validated against the classical Euler solution based on the equivalent bending rigidity.

Table 2.. Convergence of the Navier-series solution with respect to the maximum retained mode number.

Maximum retained Navier mode	Mid-span deflection (mm)	Relative change (%)
1	0.40860	--
3	0.40692	0.41387
5	0.40705	0.03227
7	0.40703	0.00603
9	0.40703	0.00173
11	0.40703	0.00064

As listed in Table 2, the calculated mid-span deflection converges rapidly as the number of retained Navier terms increases. The maximum difference between the single-term approximation and the converged solution is less than 0.4%, indicating that the proposed formulation exhibits excellent numerical stability. After five Navier terms, the relative variation becomes negligible, confirming that the solution has practically converged. Therefore, five Navier terms were adopted in all subsequent analyses to ensure an appropriate balance between computational efficiency and numerical accuracy.

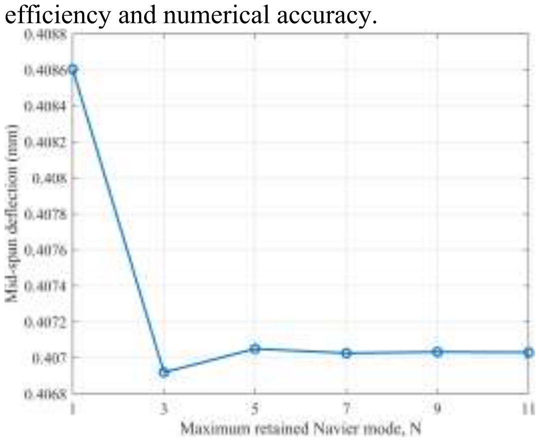

Fig. 7. Convergence of the mid-span deflection with increasing maximum retained Navier mode.

Fig.7 clearly demonstrates that the proposed Navier-series solution converges rapidly. Increasing the number of retained modes beyond five produces almost no visible change in the predicted deflection. Consequently, the numerical cost can be significantly reduced without sacrificing solution accuracy.

3.1.1. Model Validation

To further verify the accuracy of the proposed formulation, the predicted critical buckling load was compared with the classical Euler buckling solution using the equivalent bending rigidity of the sandwich beam. The equivalent bending rigidity was calculated by integrating the effective Young's modulus through the beam thickness. This comparison provides an independent verification of the developed TSDT–Navier implementation before conducting the thermo-mechanical parametric investigations.

Table 3. Validation of the present buckling formulation against the equivalent Euler solution.

Method	Critical buckling load (N)
Equivalent Euler solution	31.579
Present TSDT–Navier model	31.572
Relative difference (%)	0.0196

As presented in Table. 3, the developed formulation predicts a critical buckling load of 31.572 N, whereas the equivalent Euler solution gives 31.579 N. The relative difference is only 0.0196%, demonstrating excellent agreement between the two approaches. This result confirms the correctness of the equivalent bending rigidity evaluation, the stiffness formulation, and the eigenvalue solution employed in the present numerical model.

The first buckling mode was found to be critical and was therefore adopted in all subsequent parametric analyses.

3.2. Effect of GPL Volume Fraction

The effect of GPL reinforcement on the mechanical performance of the equivalent casing model was investigated by varying the mean GPL volume fraction in the face sheets from 0 to 1%. The auxetic-core parameters, sandwich geometry, and loading conditions were maintained unchanged. The normalized mid-span deflection and critical buckling load were selected as representative indicators to evaluate the contribution of graphene reinforcement to the bending stiffness and stability characteristics.

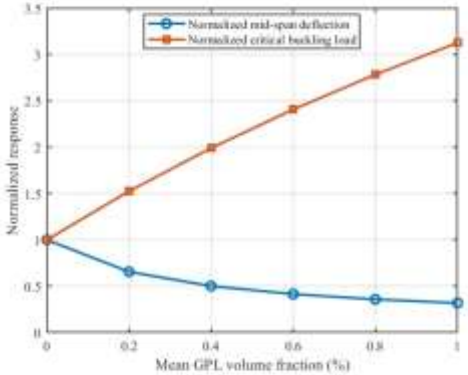

Fig. 8. Effect of GPL volume fraction on the normalized mid-span deflection and critical buckling load.

As shown in Fig.8, increasing the GPL volume fraction results in a continuous reduction in the normalized mid-span deflection and a simultaneous increase in the normalized critical buckling load. Increasing the GPL content from 0 to 1% reduces the deflection by approximately 68%, indicating a significant enhancement of the bending stiffness of the sandwich beam. This improvement is attributed to the high Young's modulus of graphene platelets and their effective contribution when embedded within the outer face sheets.
A similar strengthening trend is observed for the buckling response. The critical load increases by approximately 212% when the GPL volume fraction increases from 0 to 1%. Since the face sheets are located away from the neutral axis, the enhanced longitudinal stiffness of the GPL-reinforced layers produces a considerable increase in the equivalent bending rigidity, resulting in improved resistance against global buckling.

3.3. Effect of GPL Distribution Pattern

Although the overall GPL volume fraction is the primary factor governing the stiffness enhancement of GPLRC face sheets, the spatial distribution of graphene platelets through the thickness also affects the structural response. To evaluate this influence, three commonly adopted distribution patterns, namely UD, FG-X, and FG-O, were investigated while maintaining the same mean GPL volume fraction, beam geometry, auxetic-core configuration, and loading conditions.

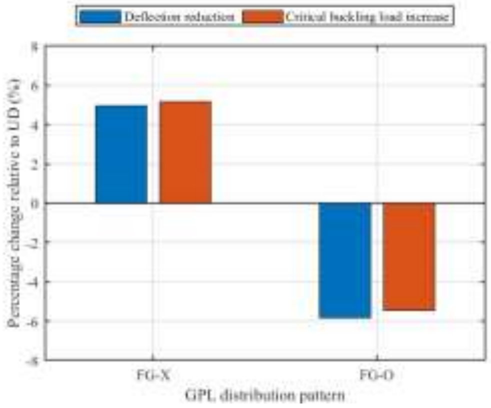

Fig. 9. Relative changes in mid-span deflection and critical buckling load for different GPL distribution patterns.

As shown in Fig.9, the FG-X distribution provides the best structural performance, reducing the mid-span deflection by approximately 5% and increasing the critical buckling load by about 5% compared with the uniform distribution. In contrast, the FG-O pattern slightly deteriorates both responses.
The improved behavior of the FG-X configuration is attributed to the concentration of GPLs near the outer surfaces of the face sheets, where bending stresses are the highest. Consequently, the bending stiffness is utilized more efficiently than in the UD and FG-O configurations. Therefore, the FG-X distribution is adopted in the subsequent thermo-mechanical analyses.

3.4. Effect of Auxetic Cell Angle on the Structural Response

Fig.10 illustrates the influence of the auxetic cell angle on the bending and buckling behavior of the equivalent GPLRC–auxetic sandwich beam under geomechanical loading. As the cell angle changes from −15° to −45°, the normalized mid-span deflection gradually increases, whereas the normalized critical buckling load decreases. This trend is primarily attributed to the reduction in the longitudinal stiffness of the auxetic core E_{11} as the magnitude of the negative cell angle increases.

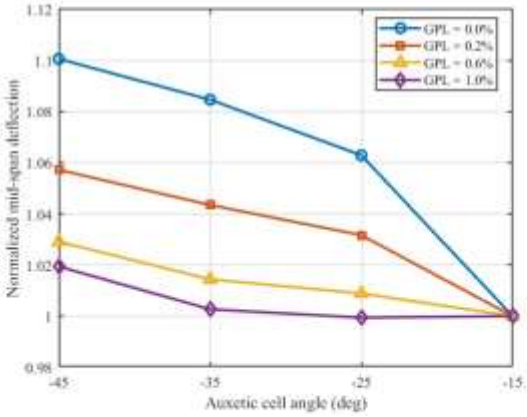

Fig. 10a. Effect of the auxetic cell angle on the structural response of the equivalent GPLRC–auxetic sandwich beam under geomechanical loading.

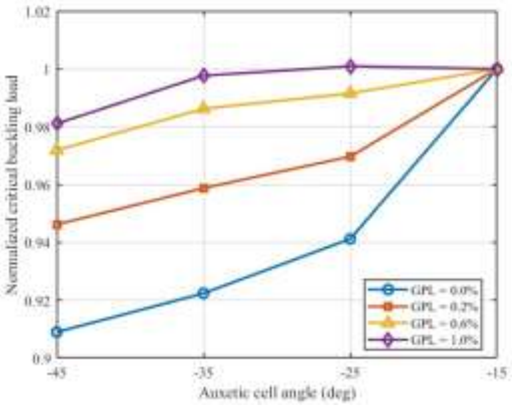

Fig. 10b. Normalized critical buckling load for different GPL volume fractions

The influence of the cell angle is most pronounced in the unreinforced beam. For the case without GPL reinforcement $V_{GPL} = 0\%$, increasing the cell angle from $-15°$ to $-45°$ increases the mid-span deflection from 1.2227 mm to 1.3457 mm, corresponding to an increase of approximately 10.1%. Simultaneously, the critical buckling load decreases from 45.8 kN to 41.6 kN, representing a reduction of approximately 9.1%.
As the GPL volume fraction increases, the sensitivity of the structural response to the auxetic cell angle becomes progressively smaller. At 1.0 vol.% GPL, the same variation in cell angle changes the mid-span deflection by less than 2%, while the corresponding variation in the critical buckling load is also below 2%. These results indicate that the increased stiffness provided by the graphene-reinforced face sheets effectively compensates for the reduction in the longitudinal stiffness of the auxetic core.

Overall, the combined results demonstrate that graphene reinforcement not only enhances the global bending stiffness and buckling resistance of the equivalent casing model but also reduces its dependence on the geometric configuration of the auxetic core. Consequently, sandwich beams with higher GPL contents exhibit greater structural stability and lower sensitivity to manufacturing variations in the auxetic cell geometry.

3.5. Effect of Geomechanical Loading on Structural Safety

The influence of geomechanical loading on the structural response of the equivalent GPLRC–auxetic sandwich beam was investigated by gradually increasing the effective external pressure while maintaining all geometric and material parameters unchanged. The equivalent transverse line load was determined using the proposed geomechanical loading model, whereas the corresponding bending response was obtained from the Navier–TSDT solution. Table.4 summarizes the variation of the mid-span deflection and the linear-load utilization for representative loading conditions.

Table 4. Effect of geomechanical loading on the equivalent GPLRC–auxetic sandwich beam.

External effective pressure (MPa)	Mid-span deflection (mm)	Linear-load utilization
25	0.105	0.175
35	0.316	0.526
45	0.526	0.877
50	0.631	1.052
60	0.842	1.403

As the effective external pressure increases from 25 MPa to 60 MPa, the mid-span deflection increases from 0.105 mm to 0.842 mm, indicating a nearly proportional increase in structural deformation under the applied geomechanical loading. Over the same pressure range, the deflection-to-thickness ratio rises from 0.0088 to

0.0702, demonstrating a progressive reduction in the serviceability margin of the equivalent casing. As illustrated in Fig.11, the linear-load utilization increases monotonically with increasing effective external pressure and reaches $U = 1$ at approximately 48.5 MPa. It should be emphasized that this value does not represent the collapse pressure of the actual cylindrical casing. Rather, it corresponds to the effective external pressure at which the adopted linear-response criterion, $|w_{max}|/h = 0.05$, is reached for the present reduced-order beam configuration. Accordingly, the value of 48.5 MPa should be interpreted as a model-specific limiting pressure for the assumed geometry, material configuration, boundary conditions, and loading assumptions.

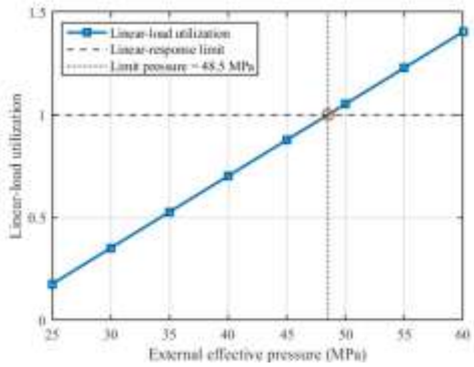

Fig. 11. Variation of the linear-load utilization with increasing external effective pressure for the equivalent GPLRC–auxetic sandwich beam. The horizontal dashed line represents the prescribed linear-response limit (U=1), while the vertical dotted line indicates the corresponding limiting external pressure..

3.6. Thermo-Mechanical Buckling Behavior under Combined Loading

The coupled effects of temperature rise and initial compressive loading on the buckling behavior of the GPL-reinforced auxetic sandwich beam were investigated. Three initial preload ratios $\mu = 0.4\,, 0.6$, and 0.8, were considered, where $\mu = N_{geo}/N_{cr,0}$ and $N_{cr,0}$ denotes the critical buckling load at the reference temperature. For each preload level, the temperature-dependent properties of the GPLRC face sheets and auxetic core, together with the compressive axial force generated by restrained thermal expansion, were incorporated into the TSDT-based buckling formulation. The temperature rise was varied from 0º to 300º to examine the interaction between thermal degradation and the initial geomechanical preload.

Fig.12 presents the variation of the thermo-mechanical buckling utilization factor with temperature rise for different initial preload levels. For all cases, the utilization factor increases with increasing temperature because of the combined effects of stiffness degradation and the additional compressive force generated by restrained thermal expansion. For preload ratios of 0.4 and 0.6, the utilization factor remains below the instability limit within the investigated temperature range. However, for $\mu = 0.8$, the utilization factor reaches unity at a temperature rise of approximately 242 °C, indicating the onset of thermo-mechanical buckling.

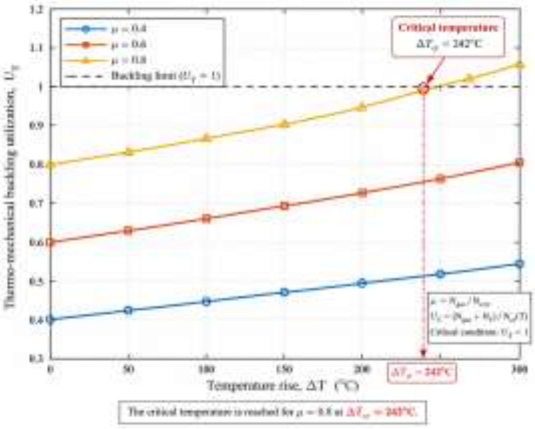

Fig. 12. Thermo-Mechanical Buckling at Critical Temperature.

These results demonstrate that the initial geomechanical preload has a significant influence on the thermal stability of the sandwich beam. Higher preload levels reduce the available buckling margin and accelerate the onset of instability under thermal loading. Therefore, casing sections operating under high in-situ compressive stresses are more vulnerable to thermo-mechanical buckling, even when the same GPLRC-auxetic sandwich configuration is employed.

4. Conclusions and recommendations

The present study developed a reduced-order analytical model for investigating the global thermo-mechanical response of an equivalent oil-well casing represented by a GPL-reinforced sandwich beam with a re-entrant auxetic core. The formulation was established using Reddy's third-order shear deformation theory, Hamilton's principle, and the Navier solution, while effective geomechanical stresses, pore-pressure effects, temperature-dependent material properties, restrained thermal expansion, and initial axial compression were incorporated to evaluate the bending and buckling responses under representative downhole loading conditions.

The parametric results showed that increasing the mean GPL volume fraction from 0 to 1% reduced the mid-span deflection by approximately 68% and increased the critical buckling load by about 212%. Among the investigated GPL distributions, the FG-X pattern provided approximately 5% lower deflection and 5% higher buckling capacity than the uniform distribution. Increasing the magnitude of the negative auxetic cell angle from 15° to 45° reduced the longitudinal stiffness of the core; however, at 1% GPL content, the resulting variations in both deflection and buckling load remained below 2%. The adopted linear-response criterion was reached at an effective external pressure of approximately 48.5 MPa for the present model configuration. This value should be interpreted as a model-specific threshold associated with the assumed geometry, material properties, boundary conditions, and linear-response criterion, rather than as the collapse pressure of an actual cylindrical casing. The thermo-mechanical analysis further showed that increasing temperature progressively reduced the available buckling margin, with the preload ratio (μ=0.8) reaching the instability condition at a temperature rise of approximately 242 °C, while the cases with (μ =0.4) and 0.6 remained below the instability limit within the investigated temperature range.

Overall, the results indicate that the combined use of GPL-reinforced face sheets and a re-entrant auxetic core can substantially modify the stiffness and global stability characteristics of the equivalent sandwich-beam model. The proposed formulation should therefore be regarded as a computationally efficient reduced-order framework for preliminary parametric assessment of selected global casing response modes, rather than as a substitute for full three-dimensional casing analysis or a direct design criterion for field applications. Further work should extend the present formulation to cylindrical shell models and include local ovalization, casing–cement–formation interaction, connection effects, geometric and material nonlinearities, cyclic thermo-mechanical loading, and experimental or high-fidelity numerical validation before direct application to practical casing design.

5. References

[1] Wu, X., Zhang, X., Liu, H., & Li, Y. (2021). Study on thermo-hydro-mechanical coupling and the stability of a geothermal wellbore structure. Energies, 14(3), 649. DOI: 10.3390/en14030649.

[2] Papanastasiou, P., & Zervos, A. (2004). Wellbore stability analysis: From linear elasticity to post-bifurcation modeling. International Journal of Geomechanics, 4(1), 2–13. DOI: 10.1061/(ASCE)1532-3641(2004)4:1(2).

[3] Ghasemzadeh, H., Rahimi, E., & Iranmanesh, M. A. (2024). Analysis of the stability of open-hole multilateral wells with consideration of intermediate principal stress. Journal of Petroleum Geomechanics, 7(4), 1–14. DOI: 10.22107/jpg.2025.488426.1244.

[4] Nguyen, N. V., Nguyen-Xuan, H., Nguyen, T. N., Kang, J., & Lee, J. (2021). A comprehensive analysis of auxetic honeycomb sandwich plates with graphene nanoplatelets reinforcement. Composite Structures, 259, 113213. DOI: 10.1016/j.compstruct.2020.113213.

[5] Lieu, P. V., Zenkour, A. M., & Luu, G. T. (2024). Static bending and buckling of FG sandwich nanobeams with auxetic honeycomb core. European Journal of Mechanics - A/Solids, 103, 105181. DOI: 10.1016/j.euromechsol.2023.105181.

[6] Prawoto, Y. (2012). Seeing auxetic materials from the mechanics point of view: A structural review on the negative Poisson's ratio. Computational Materials Science, 58, 140–153. DOI: 10.1016/j.commatsci.2012.02.012.

[7] Xu, H. H., Zhang, X. G., Han, D., Jiang, W., Zhang, Y., Luo, Y. M., Ni, X. H., Teng, X. C., Xie, Y. M., & Ren, X. (2024). Mechanical characteristics of auxetic composite honeycomb sandwich structure under bending. AI in Civil Engineering, 3, 8. DOI: 10.1007/s43503-024-00026-6.

[8] Ibrahim, A., Klopocinska, A., Horvat, K., & Abdel Hamid, Z. (2021). Graphene-based nanocomposites: Synthesis, mechanical properties, and characterizations. Polymers, 13(17), 2869. DOI: 10.3390/polym13172869.

[9] Tam, M., Yang, Z., Zhao, S., & Yang, J. (2019).

Vibration and buckling characteristics of functionally graded graphene nanoplatelets reinforced composite beams with open edge cracks. Materials, 12(9), 1412. DOI: 10.3390/ma12091412.

[10] Arefi, M., & Najafitabar, F. (2021). Buckling and free vibration analyses of a sandwich beam made of a soft core with FG-GNPs reinforced composite face-sheets using Ritz method. Thin-Walled Structures, 158, 107200. DOI: 10.1016/j.tws.2020.107200.

[11] Wang, Z. X., Shen, H. S., & Shen, L. (2021). Thermal postbuckling analysis of sandwich beams with functionally graded auxetic GRMMC core on elastic foundations. Journal of Thermal Stresses, 44(12), 1479–1494. DOI: 10.1080/01495739.2021.1994902.

[12] Chen, X., Shen, H. S., & Huang, X. H. (2022). Thermo-mechanical postbuckling analysis of sandwich plates with functionally graded auxetic GRMMC core on elastic foundations. Composite Structures, 279, 114796. DOI: 10.1016/j.compstruct.2021.114796.

[13] Chen, X., Shen, H. S., & Xiang, Y. (2022). Thermo-mechanical postbuckling analysis of sandwich cylindrical shells with functionally graded auxetic GRMMC core surrounded by an elastic medium. Thin-Walled Structures, 171, 108755. DOI: 10.1016/j.tws.2021.108755.

[14] Tornabene, F., Fantuzzi, N., Bacciocchi, M., & Viola, E. (2020). Nonlinear vibration of functionally graded graphene nanoplatelet polymer nanocomposite sandwich beams. Applied Sciences, 10(16), 5669. DOI: 10.3390/app10165669.

[15] Çalık, A. (2026). Buckling and near-critical post-buckling of sandwich cylindrical shells with FG-GNP face sheets and an auxetic core under external pressure in a thermal environment: A closed-form approach. Continuum Mechanics and Thermodynamics, 38, 21. DOI: 10.1007/s00161-026-01453-9.

[16] Lakes, R. S. (1987). Foam structures with a negative Poisson’s ratio. Science, 235(4792), 1038–1040. DOI: 10.1126/science.235.4792.1038.

[17] Gibson, L. J., & Ashby, M. F. (1997). Cellular Solids: Structure and Properties (2nd ed.). Cambridge University Press. DOI: 10.1017/CBO9781139878326